Electronic Supplementary Material (ESI) for Journal of Materials Chemistry C.
This journal is © The Royal Society of Chemistry 2015

Supporting Information

Tuning the Ambipolar Charge Transport Properties of N-heteropentacenes by Their Frontier Molecular Orbital Energy Levels

Ke Liu,[a] Cheng-Li Song,[c] Ye-Cheng Zhou,[a] Xing-Yu Zhou,[a] Xiao-Jun Pan,[b] Lu-Ya Cao,[a] Cheng Zhang,[a] Yu Liu,[a] Xiong Gong,[d] and Hao-Li Zhang*[a]

[a] State Key Laboratory of Applied Organic Chemistry (SKLAOC), College of Chemistry and Chemical Engineering, Key Laboratory of Special Function Materials and Structure Design, Ministry of Education, Lanzhou University, Lanzhou, 730000, China
[b] School of Physical Science and Technology, Lanzhou University, Lanzhou, 730000, China
[c] State Key Laboratory for Oxo Synthesis & Selective Oxidation, Lanzhou Institute of Chemical Physics, CAS, Lanzhou 730000, China
[d] Department of Polymer Engineering, College of Polymer Science and Engineering, The University of Akron, Akron, Ohio 44236, United States

Correspondence Authors:

H.-L. Zhang: Haoli.zhang@lzu.edu.cn

Table of Contents

1. General methods

Instrument: ^{1}H NMR and ^{13}C NMR were recorded on a Bruker ADVANCE III 400MHz at room temperature. The ^{1}H and ^{13}C chemical shifts (δ) are reported in parts per million and the TMS is used as an internal standard. Mass spectral data (MS) were obtained on a Bruker esquire6000 mass spectrometer with ESQ6K operator. Elemental analysis data were obtained at Elementar Analysensysteme GmbH varioEL cube superuser. Melting points were recorded (uncorrected) on a Thomas–Hoover Capillary Melting Point Apparatus. UV–vis absorption spectra were measured using a TU-1810 UV–Vis spectrometer. Single crystal X-ray diffraction measurements were made on an Agilent Technologies SuperNova Eos Dual System with a Cu microfocus source and focusing multilayer optics.

2. Synthesis and characterization of the molecules

Materials: All Chemical reagents and solvents were purchased from Aldrich Chemical Co, TCI America, J&K or Alfa Aesar and were used as received without further purification unless otherwise noted.

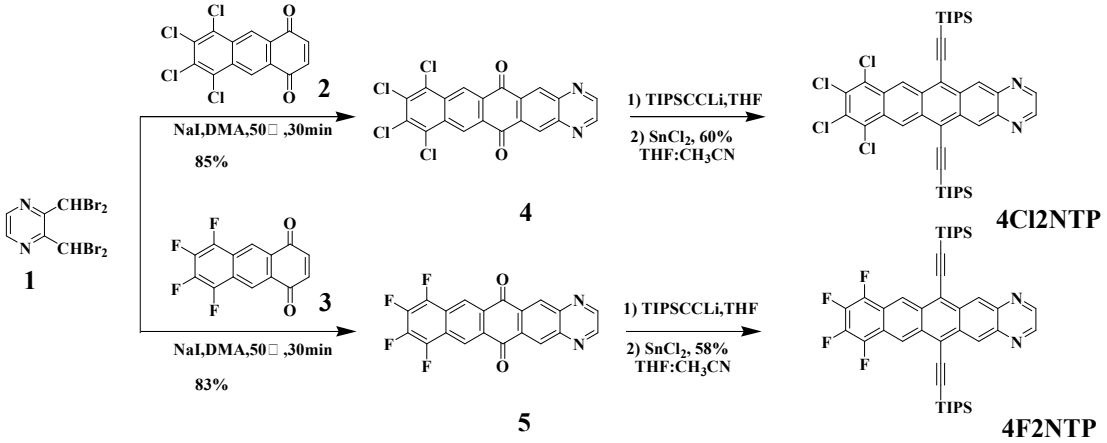

Scheme S1. Synthetic Route to 4Cl2NTP and 4F2NTP

The compound TP was synthesized according to the literature method.[1] The N-heteropentacenes 1NTP, 2NTP, 4F1NTP and 4Cl1NTP were synthesized as we reported previously.[2, 3] 2,3-bis(dibromomethyl)pyrazine (1), 5,6,7,8-tetrafluoro-1,4-anthraquinone (2) and 5,6,7,8-tetrachloro-1,4-anthraquinone (3) were synthesized following the literature procedures. The structures of the molecules were confirmed

by ^{1}H NMR and ^{13}C NMR and mass spectral data (MS).

8, 9, 10, 11-tetrachloroanthra[2,3-g]quinoxaline-6,13-dione (4):

In an oven-dried 2-necked flask, 3.00 g of sodium iodide (20.00 mmol, 5 eq) was added to a solution of 1.68 g of 2,3-bis(dibromomethyl)pyrazine (4.00 mmol, 1 eq) and 1.39 g of 5,6,7,8-tetrachloro-1,4-anthraquinone (4.00 mmol, 1 eq) in 40 mL anhydrous DMA (N,N-Dimethylacetamide). The mixture was heated and stirred at 40 °C for 1 h. After cooling to room temperature, the precipitated was filtered, washed with water and acetone and dried under vacuum. Compound 4 was obtained as a yellow solid (1.54 g, 3.40 mmol, 85%). Mp＞320 °C. This compound is very insoluble, such that even proton NMR could not be measured. MS (APCI, m/z): $[M + H]^+$ calcd for $C_{20}H_6Cl_4N_2O_2$, 448.09; found, 449.20. Anal. Calcd for $C_{20}H_6Cl_4N_2O_2$: C, 53.61; H, 1.35; N, 6.25 Found: C, 53.21; H, 1.30; N, 5.97.

8, 9, 10, 11-tetrafluoroanthra[2,3-g]quinoxaline-6,13-dione (5):

Compound 5 was prepared by the reaction of 1.68 g 2,3-bis(dibromomethyl)pyrazine (4.00 mmol, 1 eq) and 1.12 g 5,6,7,8-tetrafluoro-1,4-anthraquinone (4.00 mmol, 1 eq). Compound 5 with the similar procedure as the synthesis of compound 4 was obtained as a pale yellow solid (1.28 g, 3.32 mmol, 83%). Mp＞320 °C. This compound is very insoluble, such that even proton NMR could not be measured. MS (APCI, m/z): $[M + H]^+$ calcd for $C_{20}H_6F_4N_2O_2$, 383.27; found, 383.30. Anal. Calcd for $C_{20}H_6F_4N_2O_2$: C, 62.84; H, 1.58; N, 7.33 Found: C, 62.49; H, 1.56; N, 7.04.

8,9,10,11-tetrachloro-6,13-bis(2-(triisopropylsilyl)ethynyl)anthra[2,3-g]quinoxaline (4Cl2NTP):

In an oven-dried 2-necked flask, 1.65 mL triisopropylsilylacetylene (6.60 mmol, 4.40 M, 6.6 eq) and dry THF (20 mL) were added, then 2.0 mL n-BuLi (2.5 M in hexanes, 5.0 mmol, 5 eq) was added drop wise to this stirring solution at 0 °C under argon. This reaction was stirred for an additional 45 min at 0 °C, then 452 mg compound 4 (1 mmol, 1eq) was added, followed by 30 mL of dry THF to this solution.

The mixture was heated to 65.5 °C and stirred for 6 hrs. The system was quenched with saturated NH_4Cl aqueous solution and organic constituent was extracted with ethyl acetate (3×100 mL), washed with saturated ammonium chloride (2×100 ml) and dried with anhydrous Na_2SO_4. After evaporation of the solvent, the residue was filtered over silica gel using petroleum/ethyl acetate (v/v, 8:1) to yield the corresponding diol (635 mg, 0.78 mmol, 78%). ^{1}H-NMR (400MHz, $CDCl_3$) δ: 8.89(s, 2H), 8.95(s, 2H), 9.20(s, 2H), 5.01(s, 2H), 1.24-1.25 (42H). ^{13}C-NMR (100 MHz, $CDCl_3$) δ: 146.38, 143.03, 139.86, 138.73, 131.59, 130.95, 130.24, 129.34, 125.62, 104.10, 94.47, 71.82, 19.05, 11.58. MS (APCI, m/z): $[M-OH]^+$ calcd for $C_{42}H_{50}Cl_4N_2O_2Si_2$, 795.84; found, 795.50. Anal. Calcd for $C_{42}H_{50}Cl_4N_2O_2Si_2$: C, 62.06; H, 6.20; N, 3.45. Found: C, 62.04; H, 6.21; N, 3.09.

The crude diol was recrystallized with hexane to yield a write solid. The corresponding 252 mg diol (0.31 mmol, 1 eq) was dissolved in dry THF: CH_3CN=1:1 (60 mL) and 710 mg $SnCl_2$ (3.72 mmol, 12 eq) under argon. The mixture was heated at 60 °C for 1 h. After cooling to room temperature, saturated brine (20 mL) and triethylamine (2 mL) was added to the mixture and organic constituent was extracted with dichloromethane (3×100 mL), and washed the organic phase with water (3× 100 mL). The organic layers were dried with anhydrous Na_2SO_4 and solvent was removed and the solids were further purified by chromatography on silica gel using petroleum/ dichloromethane (v/v, 1:1) solvent mixture. 4Cl2NTP was obtained as a deep blue solid (186 mg, 0.24 mmol, 60%). Mp＞320 °C; ^{1}H-NMR (400MHz, $CDCl_3$) δ: 8.89 (s, 2H), 9.56 (s, 2H), 9.79 (s, 2H), 1.35-1.36 (42H). ^{13}C-NMR (100 MHz, CDCl3) δ: 147.40, 140.15, 132.96, 131.60, 130.87, 129.93, 129.31, 128.59, 126.40, 120.72, 110.52, 103.40, 19.23, 11.80. MS (APCI, m/z): $[M+H]^+$ calcd for $C_{42}H_{48}Cl_4N_2Si_2$, 778.83; found, 779.50. Anal. Calcd for $C_{42}H_{48}Cl_4N_2Si_2$: C, 64.77; H, 6.21; N, 3.60. Found: C, 64.42; H, 6.17; N, 3.44.

8,9,10,11-tetrafluoro-6,13-bis(2-(triisopropylsilyl)ethynyl)anthra[2,3-g]quinoxaline (4F2NTP):

4F2NTP was prepared by the reaction of 1.65 mL triisopropylsilylacetylene (6.6 mmol, 6.6 eq) and 386 mg 8,9,10,11-tetrafluoroanthra[2,3-g]quinoxaline-6,13-dione(1 mmol, 1 eq). 4F2NTP with the similar procedure as the synthesis of 4Cl2NTP was obtained as a deep blue solid (413 mg, 0.58 mmol, 73%). The corresponding diol: ^{1}H-NMR (400MHz, $CDCl_3$) δ: 8.85(s, 2H), 8.89(s, 2H), 8.97(s, 2H), 5.38(s, 2H), 1.23 (42H). ^{13}C-NMR (100 MHz, $CDCl_3$) δ: 146.27, 142.85, 140.04, 137.62, 129.04, 120.23, 119.55, 119.46, 119.37, 104.08, 94.38, 71.79, 18.93, 11.52. MS (APCI, m/z): [M-OH] $^{+}$ calcd for $C_{42}H_{50}F_4N_2O_2Si_2$, 730.02; found, 729.70. Anal. Calcd for $C_{42}H_{50}F_4N_2O_2Si_2$: C, 67.53; H, 6.75; N, 3.75. Found: C, 67.51; H, 6.67; N, 3.54. Compound 2: Mp＞320 °C; ^{1}H-NMR (400MHz, $CDCl_3$) δ: 8.88 (s, 2H), 9.53 (s, 2H), 9.60 (s, 2H), 1.34-1.36 (42H). ^{13}C-NMR (100 MHz, CDCl3) δ: 147.38, 140.12, 132.64, 130.92, 129.26, 120.86, 120.46, 120.17, 120.07, 119.97, 110.49, 103.34, 19.14, 11.77. MS (APCI, m/z): [M + H] $^{+}$ calcd for $C_{42}H_{48}F_4N_2Si_2$, 713.01; found, 713.70. Anal. Calcd for $C_{42}H_{48}F_4N_2Si_2$: C, 70.75; H, 6.79; N, 3.93. Found: C, 70.53; H, 6.62; N, 3.72.

3. Spectroscopic properties

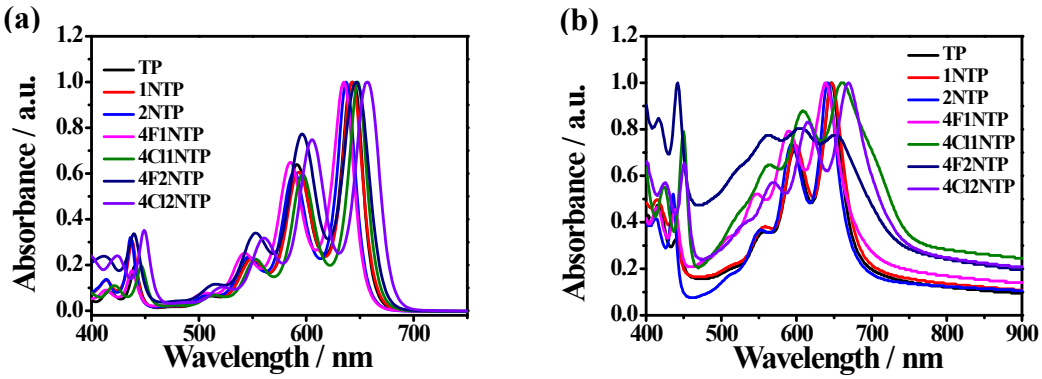

Figure S1. Normalized UV-vis absorption spectra (a) recorded in dilute toluene solution and (b) recorded on the thin films on quartz substrates of all the N-heteropentacene derivatives.

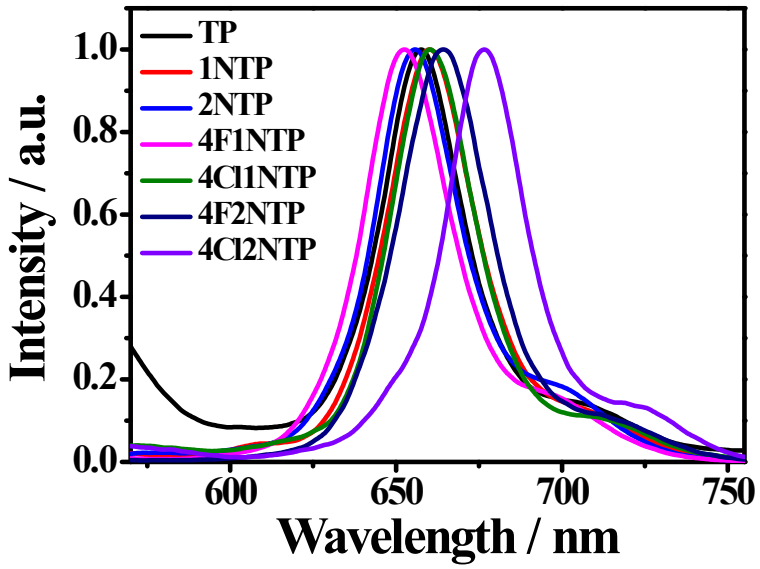

Figure S2. Normalized fluorescence emission spectra recorded in a dilute toluene solution of all the N-heteropentacene derivatives.

4. Stability

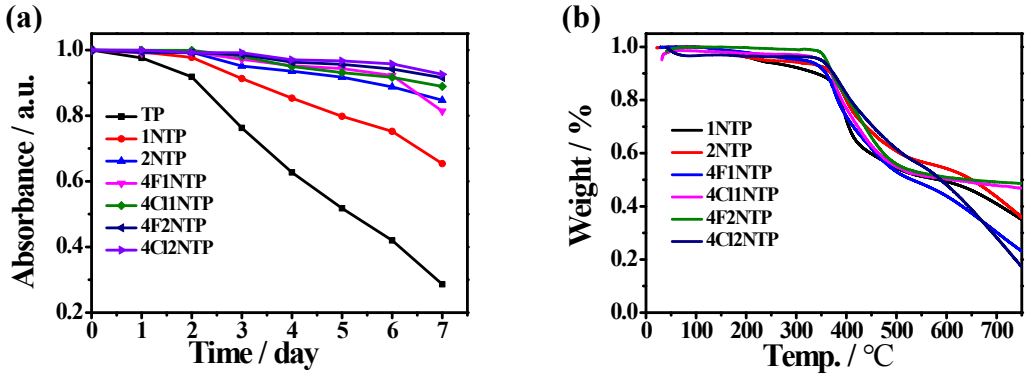

Figure S3. The photo-stability (a) and thermal stability (b) of all the N-heteropentacene derivatives were shown.

5. X-ray diffraction patterns and AFM images

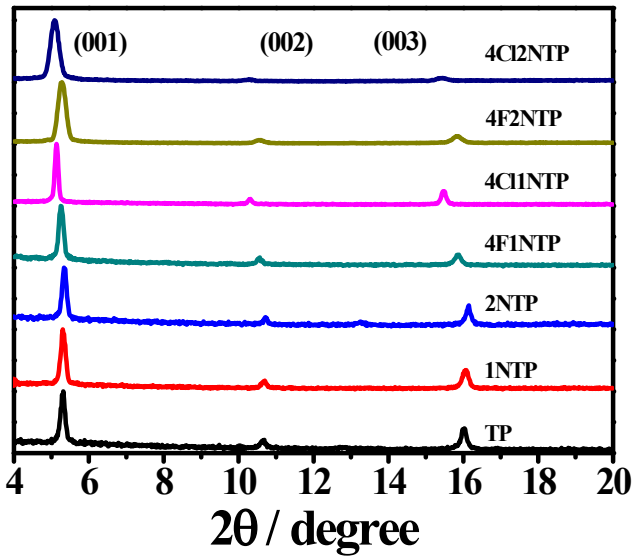

Figure S4. X-ray diffraction patterns of all the N-heteropentacene derivatives thin films deposited on OTMS-treated SiO_2 at T_{sub} = 60 °C (film thickness: 50 nm).

Table S1. Summary of Bragg diffraction angles (2θ, °) and d-spacing (d, nm) of the thin films and single crystals from Diamond 3.0 program for all the N-heteropentacene derivatives

Mol.	Thin films						Single crystals								
	$2\theta_1$	d_1	$2\theta_2$	d_2	$2\theta_3$	d_3	$2\theta_1$	d_1	*hkl*	$2\theta_2$	d_2	*hkl*	$2\theta_3$	d_3	*hkl*
TP	5.32	1.66	10.66	0.83	16.05	0.55	5.35	1.65	001	10.72	0.82	002	16.11	0.55	003
1NTP	5.31	1.66	10.69	0.83	16.10	0.55	5.34	1.65	001	10.70	0.83	002	16.07	0.55	003
2NTP	5.35	1.65	10.71	0.83	16.14	0.55	5.38	1.64	001	10.77	0.82	002	16.19	0.55	003
4F1NTP	5.24	1.69	10.53	0.84	15.85	0.56	5.28	1.67	001	10.57	0.84	002	15.89	0.56	003

4Cl1NTP	5.14	1.72	10.31	0.86	15.48	0.57	5.12	1.73	001	10.24	0.86	002	15.39	0.58	003
4F2NTP	5.25	1.68	10.52	0.84	15.87	0.56	5.29	1.67	001	10.60	0.83	002	15.92	0.56	003
4Cl2NTP	5.09	1.74	10.33	0.86	15.43	0.57	5.12	1.72	001	10.25	0.86	002	15.40	0.58	003

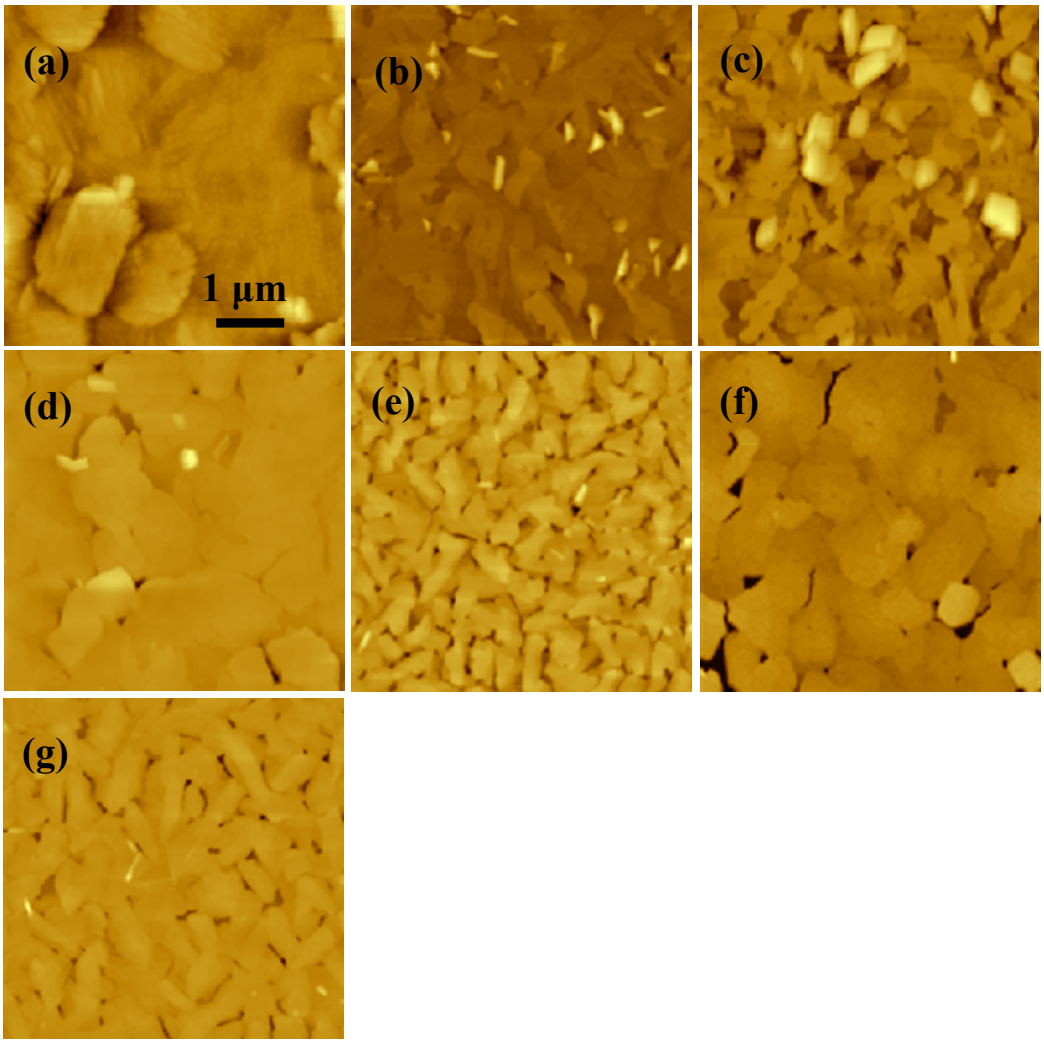

Figure S5. The AFM images of compound TP (a), 1NTP (b), 2NTP (c), 4F1NTP (d), 4Cl1NTP (e), 4F2NTP (f) and 4Cl2NTP (g) deposited on OTMS-treated SiO_2 at T_{sub} = 60 °C (film thickness: 50 nm).

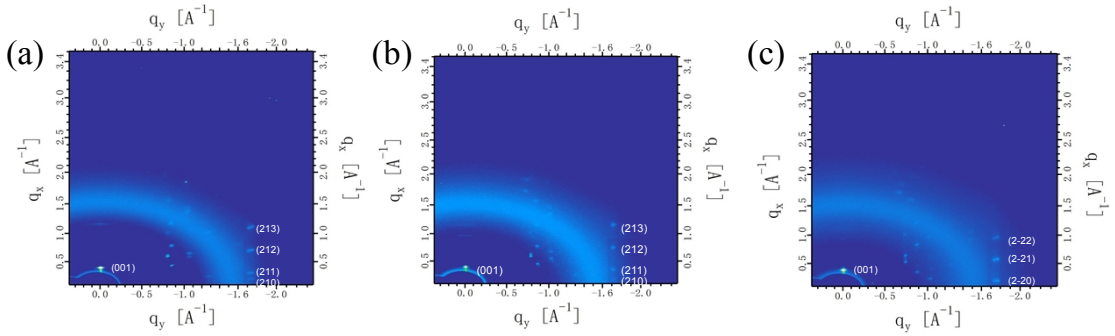

Figure S6. 2D-GIXRD patterns for thin film of 1NTP (a), 2NTP (b), and 4Cl1NTP (c) deposited on OTMS treated SiO_2 at T_{sub}=60 °C.

6. OFET characterization

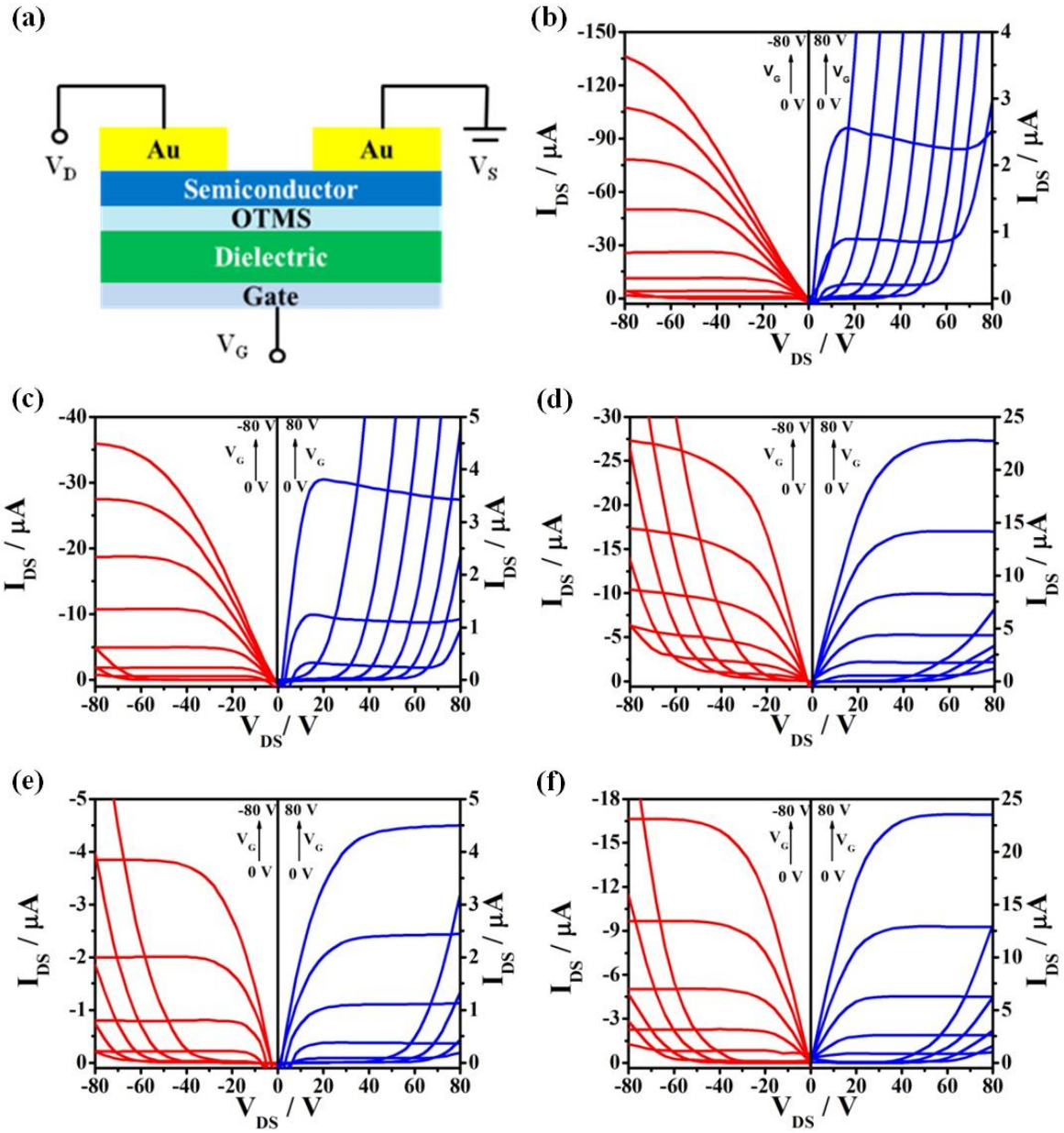

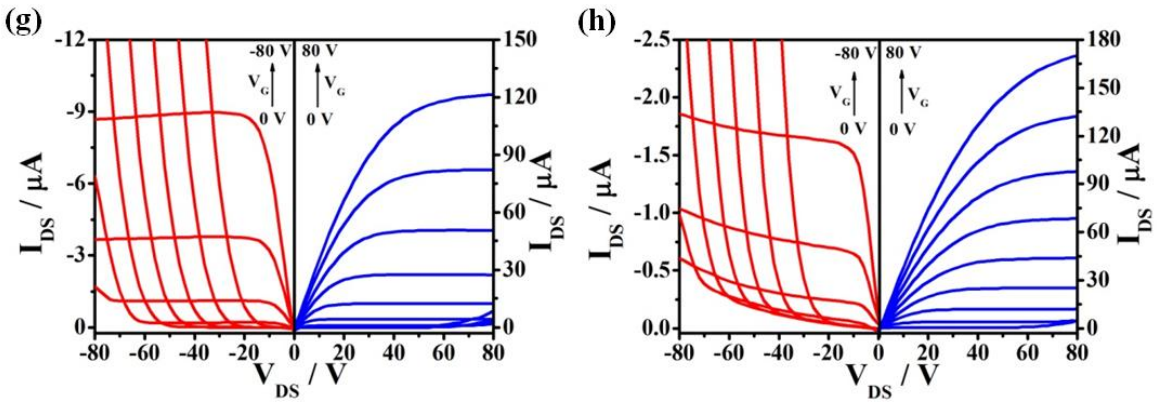

Figure S7. OFETs device structure (a), typical output curves for TP (b), 1NTP (c), 2NTP (d), 4F1NTP (e), 4Cl1NTP (f), 4F2NTP (g) and 4Cl2NTP (h) deposited on OTMS-treated SiO_2 substrates at T_{sub} = 60 °C with Au electrodes respectively.

7. Simulation of charge transport parameters

7.1 Calculation of transfer integral

The electronic coupling calculations of dimers are performed by the local density functional in the conjunction with the PW91 gradient corrections with the TZ2P basis set, as implemented in the ADF2010. Then effect charge coupling V can be calculated from the spatial overlap (S_{RP}), charge transfer integral (J_{RP}), and site energies (H_{RR},H_{PP}).[4]

$$V_{RP} = \frac{J_{RP} - S_{RP}(H_{RR} + H_{PP})/2}{1 - S_{RP}^2} \qquad \text{S(1)}$$

The parameters S_{RP}, J_{RP}, H_{RR}, and H_{PP} were needed for the calculation of V can be obtained from the software.

7.2 Calculation of reorganization energies

The definition of the intramolecular reorganization energies $\lambda_{\pm}$ is illustrated as in Fig. S8.[5-7] The reorganization energy λ_{+} (λ_{-}) for hole (electron) transport is calculated as the sum of the energy required for reorganization of the vertically ionized neutral to the cation (anion) geometry, λ_2 (λ_4), plus the energy required to reorganize the cation (anion) geometry back to the neutral equilibrium structure on the ground state potential energy surface, λ_1 (λ_3).

$$\lambda_+ = \lambda_1 + \lambda_2 \quad \text{S(2)}$$

$$\lambda_1 = E_0(Q_+) - E_0(Q_0) \quad \text{S(3)}$$

$$\lambda_2 = E_+(Q_0) - E_+(Q_+) \quad \text{S(4)}$$

$$\lambda_- = \lambda_3 + \lambda_4 \quad \text{S(5)}$$

$$\lambda_3 = E_0(Q_-) - E_0(Q_0) \quad \text{S(6)}$$

$$\lambda_4 = E_-(Q_0) - E_-(Q_-) \quad \text{S(7)}$$

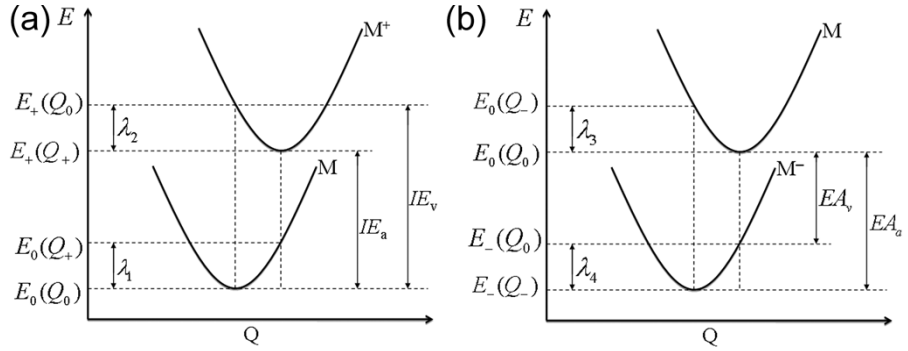

Figure S8. Sketch of the potential-energy surfaces for (a) hole transfer reaction M + $M^+ \rightarrow M^+ + M$ and (b) electron transfer reaction $M + M^- \rightarrow M^- + M$.

As suggested by Marcus equation, low reorganization energy benefits the charge transport between the molecules. On the basis, it is necessary to avoid large size or flexible functional groups, which tend to increase the reorganization energy. All the N-heteropentacene molecules studied in this work have a framework similar to TP. We studied the effect of different structure modifications on the reorganization energy, including inserting nitrogen atoms to the core and attaching halogen atoms around the periphery of the pentacene framework.

Table S2. Summary of reorganization energies (λ), vertical and adiabatic ionization energies (*IE*) and electron affinities (*EA*) (eV) for all the N-heteropentacene derivatives

Mol.	λ_+	λ_-	IE_v	IE_a	EA_v	EA_a

TP	0.139	0.200	5.984	5.914	1.894	–1.994
1NTP	0.150	0.197	6.105	6.030	1.991	–2.090
2NTP	0.161	0.190	6.228	6.147	2.085	–2.180
4F1NTP	0.173	0.206	6.386	6.300	2.264	–2.368
4Cl1NTP	0.156	0.176	6.421	6.345	2.476	–2.547
4F2NTP	0.177	0.200	6.587	6.488	2.556	–2.633
4Cl2NTP	0.162	0.178	6.529	6.451	2.606	–2.679

Tab. S2 summarizes the calculated λ, *IE*, *EA* for hole or electron transport of pentacene and the N-hereropentacenes. The hole reorganization energies of TP are calculated to be 0.139 eV, which is in good agreement with previous reports.[5, 8, 9] The reorganization energies of 1NTP and 2NTP are 0.150 and 0.161 eV for holes and 0.197 and 0.190 eV for electrons respectively. Compared to TP the reorganization energy increases with the increasing number of N atoms present in the pentacene backbone. More significant increase of the reorganization energies is found after the halogenations of the N-hereropentacenes. The hole and electron reorganization energies increased to 0.177 eV and 0.200 eV for 4F2NTP, and 0.162 eV and 0.178 eV for 4Cl2NTP respectively. Noticeably, though the reorganization energies of the N-heteropentacenes are higher than pentacene, the hole and electron reorganization energies of the N-heteropentacenes under investigation are still relatively small, suggesting that these compounds are good candidates for high performance organic semiconductor materials.[5, 10] Meanwhile, the calculation indicates that *IE* and *EA* also show trends of increase with the introduction of nitrogen and halogen atoms. The *EA* of 4Cl2NTP (−2.679 eV) is higher than that of 4F2NTP (−2.633 eV), even though Cl is less electronegative than F, suggesting that Cl atom is a more effective way to prepare n-type materials than F atom.

7.3 Simulations for mobility

Charge mobility can be obtained by simulating a diffusion process and using the Einstein relationship.[8, 11] At first we choose one molecule (*j*) as the initial charge

center randomly. And the charge hops from molecule *j* to molecule *i* with a probability:

$$P_{ij} = \frac{k_{CT}^{ij}}{\sum_{i} k_{CT}^{ij}} \qquad \text{S(8)}$$

where k_{CT}^{ij} is the hopping rate between molecule *i* and molecule *j* and with time $t = 1/k_{CT}^{ij}$. At each hopping, a random number *r* between 0 and 1 is generated. If $\sum_{i=1}^{n-1} P_{ij} < r \leq \sum_{i=1}^{n} P_{ij}$, then the charge moves from molecule *j* to molecule *n*. In every simulation, we save the time and squared displacement every 1,000,000 hoppings, and 5×10^9 hoppings are involved in every simulation. The simulated time is more than 1 μs even to 1 ms. The count hops are large enough to ensure our simulation is stable. Due to the random process, the relationship between the squared displacement and diffusion time is uncertain. In order to obtain a converged diffusion constant, as indicated by a linear relationship between the square of the diffusion distance and the diffusion time, 2400 times of simulation were performed.

From the above simulation, the diffusion constant is obtained by:

$$D = \lim_{t\to\infty} \frac{l(t)^2}{2nt} \qquad \text{S(9)}$$

where $l(t)^2$ is the mean-squared displacement of 2400 simulation, while *n* is diffusion dimension (here is 3) and *t* is the average diffusion time. Then the charge drift mobility μ from hopping is evaluated from the Einstein relation.

$$\mu = \frac{e}{k_B T} D \qquad \text{S(10)}$$

7.4 Simulation model of the single crystals

According to their single crystal structures, all the N-heteropatacenes take "brick-wall" packing, which is considered to have good orbital overlap and hence

relatively large transfer integral value. The main hopping pathways for these molecules are presented in Fig. S9 and the corresponding transfer integral values calculated by Eq. S(1) are listed in Tab. S3.

Based on the two key parameters of the reorganization energy and the transfer integral, the electronic hopping rate is computed by the Marcus equation (Eq. 1). Then the kinetic Monte Carlo simulation approach[12] is adopted to calculate the charge diffusion process based on the microscopic charge transfer rate in organic molecular single crystals. As an example, the relationship of squared displacement $l(t)^2$ and time t for the hole hopping of 4Cl2NTP is depicted in Fig. S10. Using the Einstein relation Eq. S(10), we evaluated the hole and electron mobilities of N-heteropentacene derivatives, as show in Tab. 3.

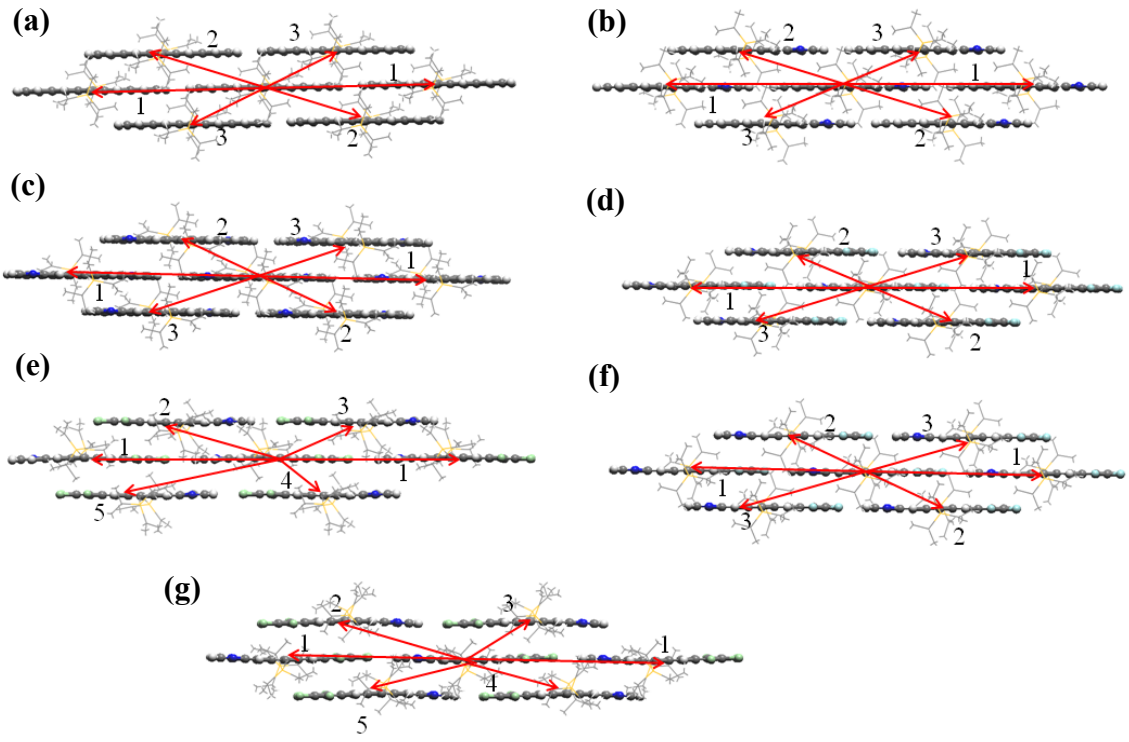

Figure S9. Molecular sacking motifs and charge transfer pathways in single crystals of TP (a), 1NTP (b), 2NTP (c), 4F1NTP (d), 4Cl1NTP (e), 4F2NTP (f) and 4Cl2NTP (g) respectively.

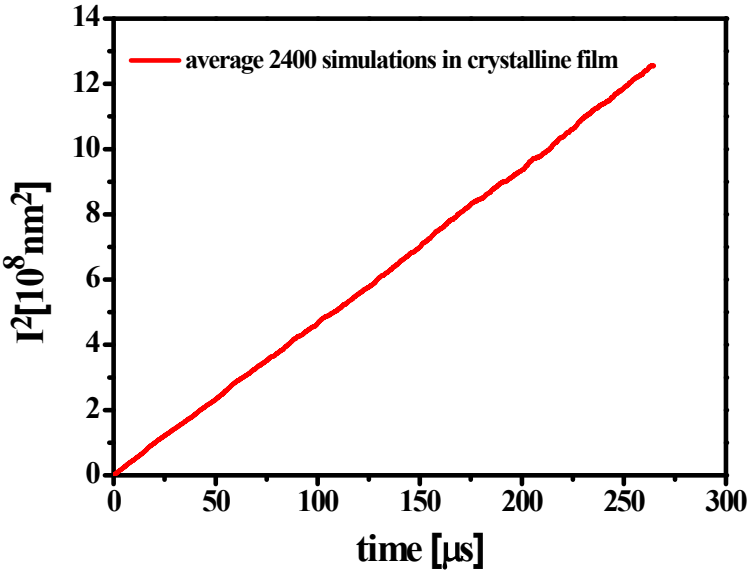

Figure S10. Squared displacement *vs* simulation time for the hole transport in the single crystals of 4Cl2NTP.

Table S3. Calculated the hole and electron transfer integrals (V_h and V_e, meV) for all the N-heteropentacene derivatives along different hopping pathways in single crystals; the mass center distance (d/Å); (*P*: the hopping pathway)

P	TP			1NTP			2NTP			4F1NTP		
	d	V_h	V_e	*d*	V_h	V_e	*d*	V_h	V_e	*d*	V_h	V_e
1	16.22	1.50	7.70	16.33	1.10	6.70	16.31	0.80	7.50	16.72	0.70	1.30
2	10.21	3.20	63.40	10.05	5.50	68.60	7.96	10.80	98.30	7.83	8.40	74.50
3	7.57	24.60	127.30	7.84	12.10	107.90	9.90	20.70	76.00	10.38	7.30	18.20

P	4Cl1NTP			4F2NTP			4Cl2NTP		
	d	V_h	V_e	*d*	V_h	V_e	*d*	V_h	V_e
1	17.35	1.70	5.30	16.61	1.00	2.80	17.11	0.80	8.20
2	9.62	52.40	67.90	7.79	14.20	101.50	12.29	5.10	31.50
3	8.2	62.	42.	10.	2.0	35.4	7.6	92.	52.

	4	00	70	33	0	0	3	50	10
4	7.58	58.00	21.60				8.12	27.90	36.70
5	12.71	2.40	9.80				9.47	60.20	72.00

7.5 Simulation model for disordered films

We first simulated the disordered morphologies with the Sorption model in Material Studio, which uses the Metropolis Monte Carlo method. Molecules were loaded in an empty box as much as the box could contain. After loading, we optimize the structure with Dreiding force field. Then, we get a unit cell with disordered molecules and assume that films consist of periodically arranged unit cell. A representative 3D model of disordered thin film is shown in Fig. S11. The periodic boundary condition will decrease the size of our model and make the calculation easy enough to bear it.

Different from the single crystals, there is no specific hoping pathway in disordered films as shown in Fig. S11. We then calculated intermolecular hopping rates between all neighboring molecules. In disordered thin film, any two neighbors within 12 Å (distance of mass centers) are taken as a dimer, and its electronic coupling is calculated.

The kinetic Monte Carlo simulation approach[12] was adopted to calculate the charge diffusion process based on the microscopic charge transfer rate in the disordered films. As an example, the relationship of squared displacement $l(t)^2$ and time t for the hole hopping of 4Cl2NTP is depicted in Fig. S12. Similar to that described above for the single crystals, the hole and electron mobilities of N-heteropentacene derivatives in disordered films were then calculated from the Eq. S(9) and S(10).

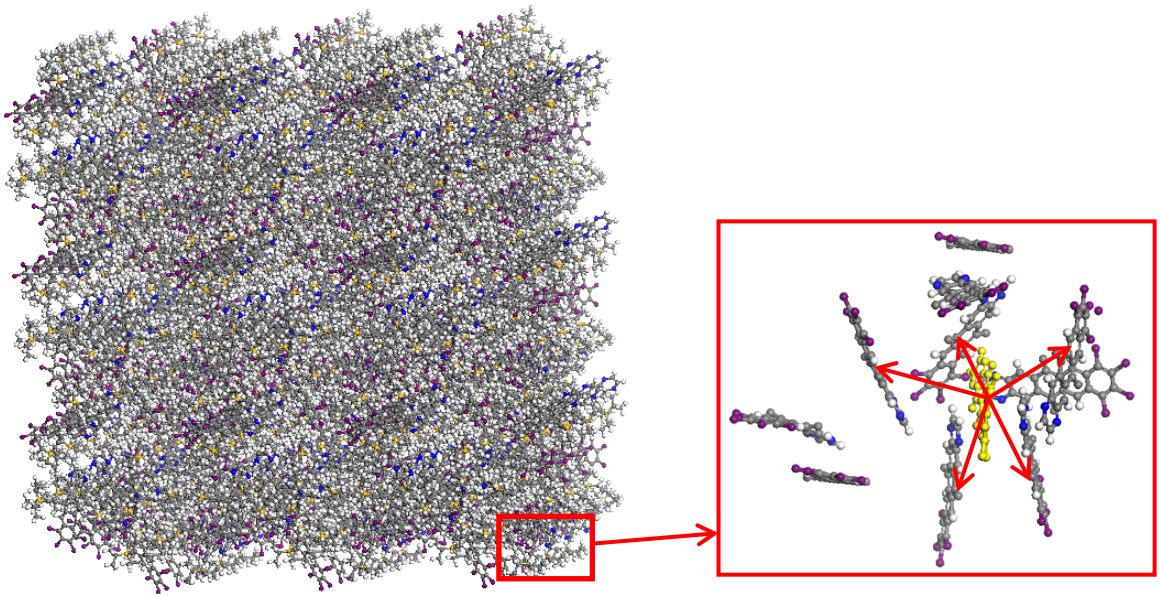

Figure S11. A representative 3D model of disordered thin film of 4Cl2NTP, formed with 3×3×3 super cell of a 40 Å unit cell, and the hopping pathways within 12 Å distance.

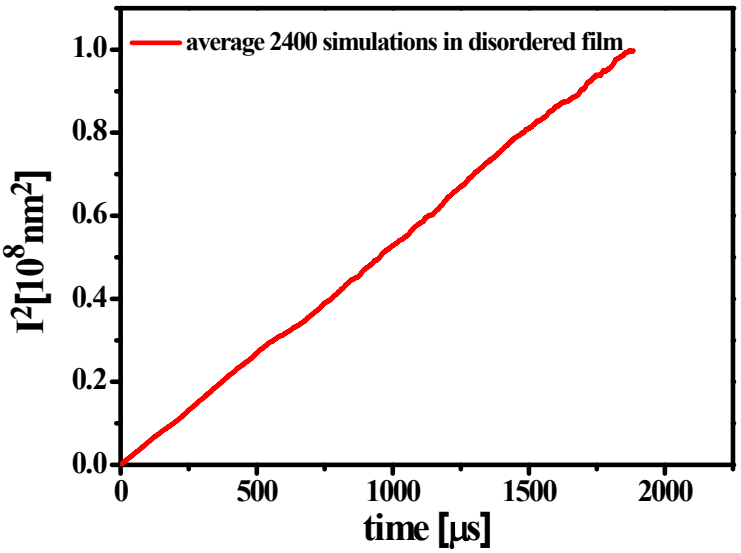

Figure S12. Squared displacement *vs* simulation time for the hole transport of 4Cl2NTP in disordered films.

8. ^{1}H NMR and ^{13}C NMR aspectra of the synthesized compounds

^{1}H NMR (400 MHz $CDCl_3$) and ^{13}C NMR (400 MHz $CDCl_3$) of 4Cl2NTP-Diol

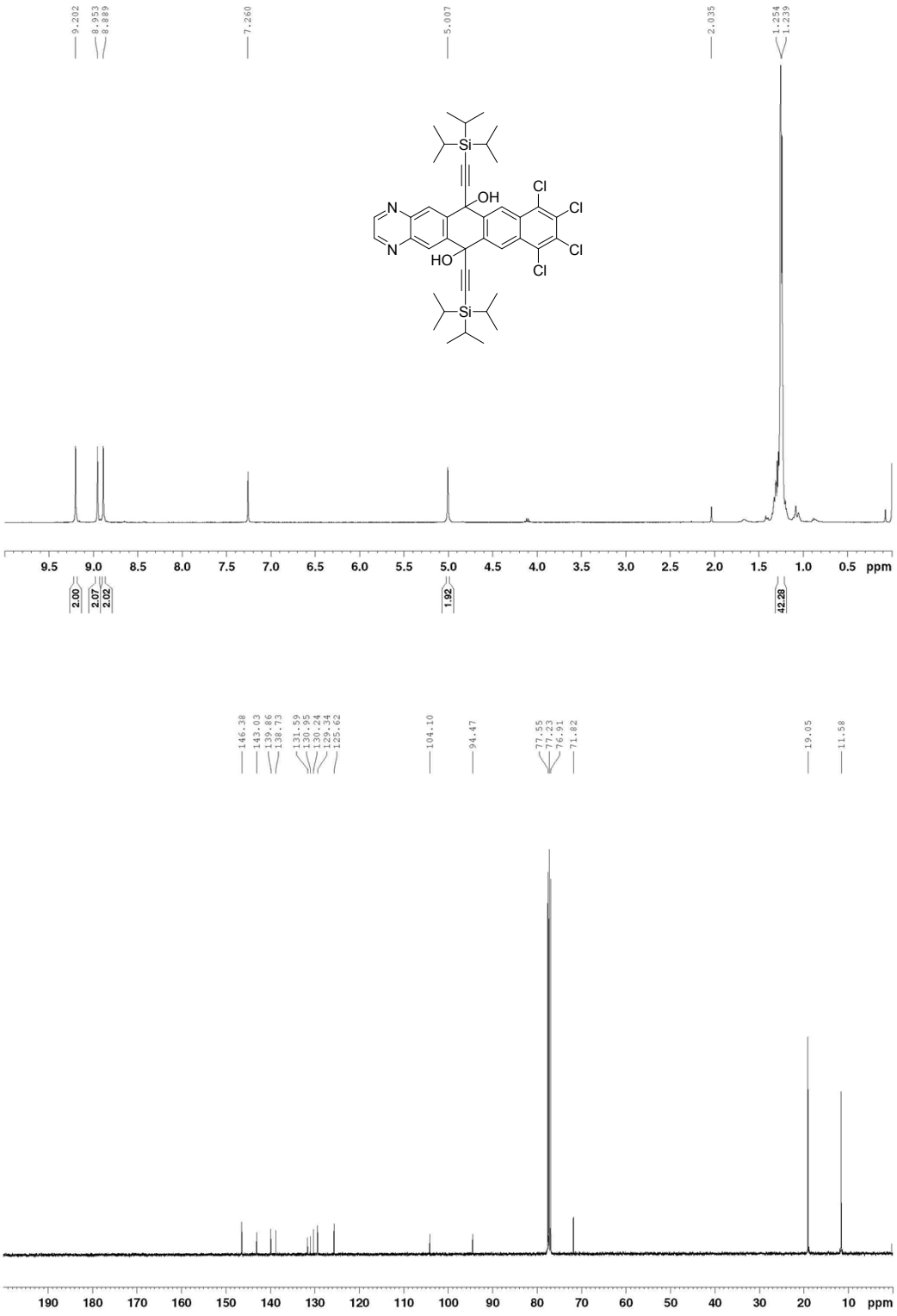

^{1}H NMR (400 MHz $CDCl_3$) and ^{13}C NMR (400 MHz $CDCl_3$) of 4Cl2NTP

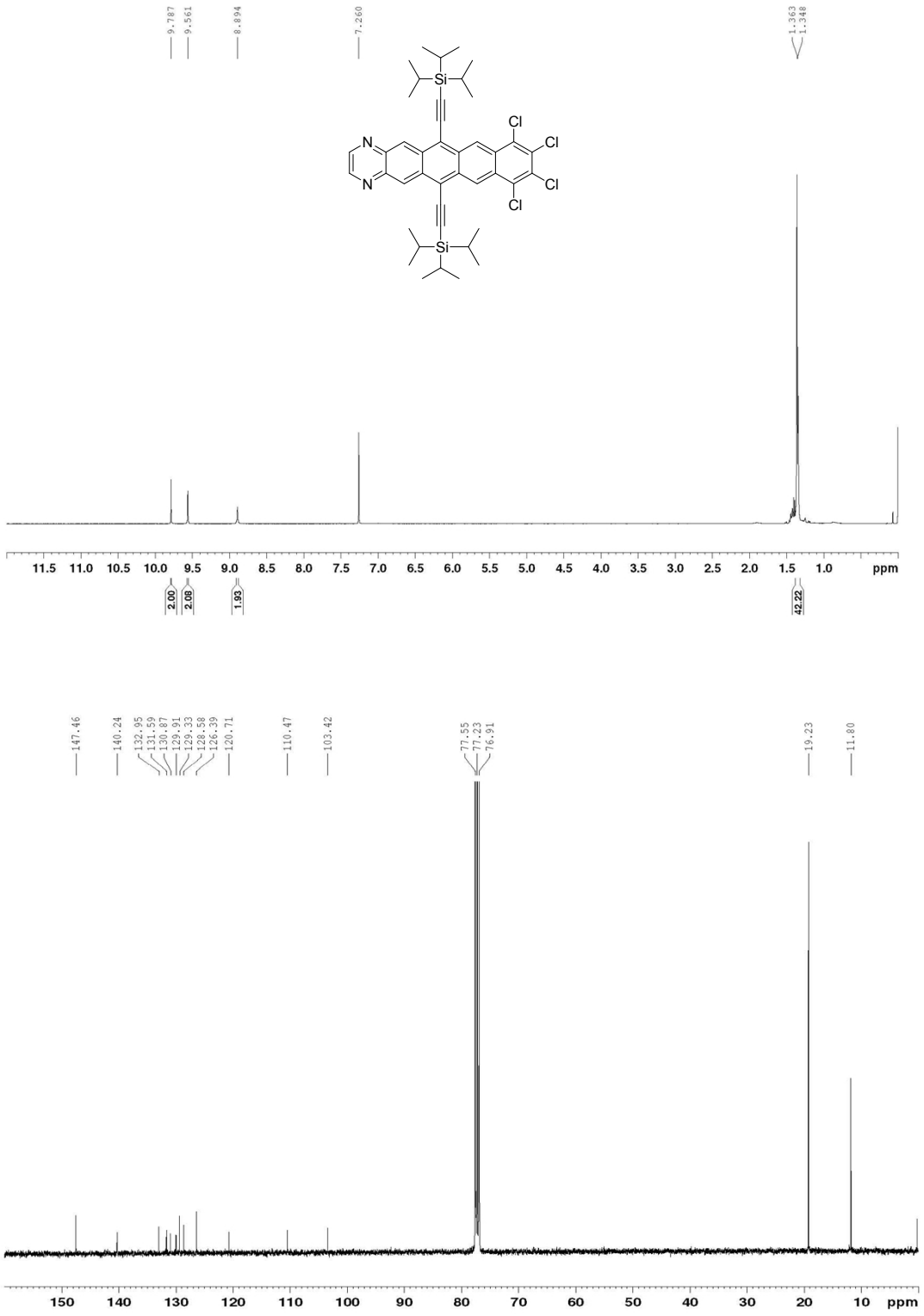

^{1}H NMR (400 MHz $CDCl_3$) and ^{13}C NMR (400 MHz $CDCl_3$) of 4F2NTP-Diol

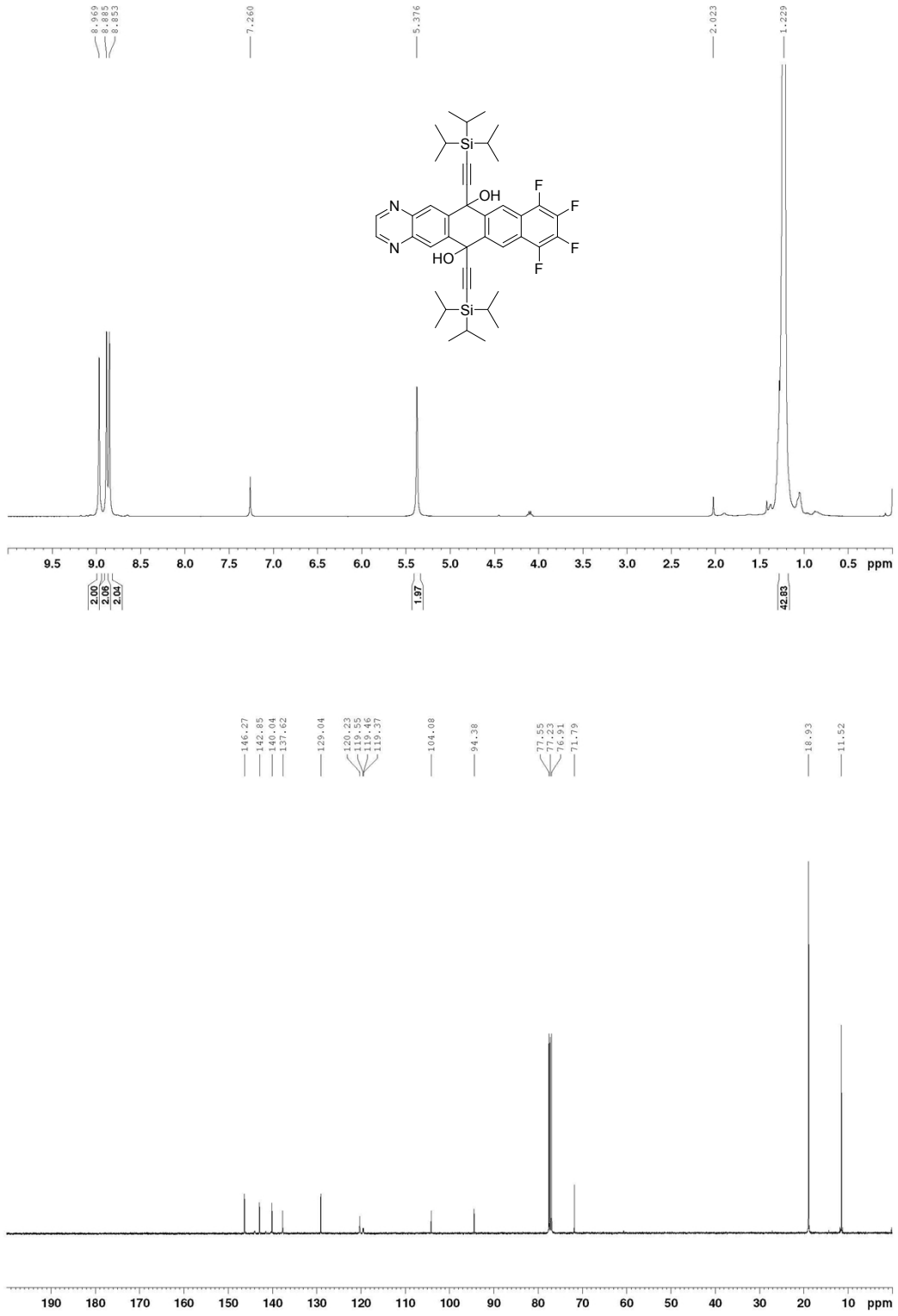

^{1}H NMR (400 MHz $CDCl_3$) and ^{13}C NMR (400 MHz $CDCl_3$) of 4F2NTP

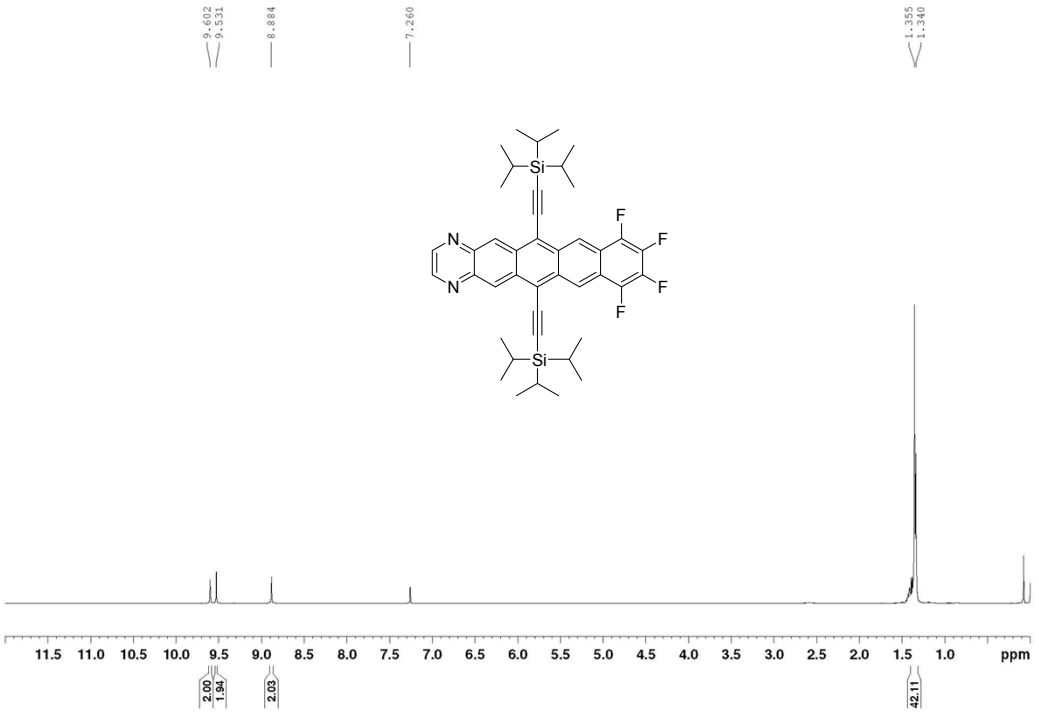

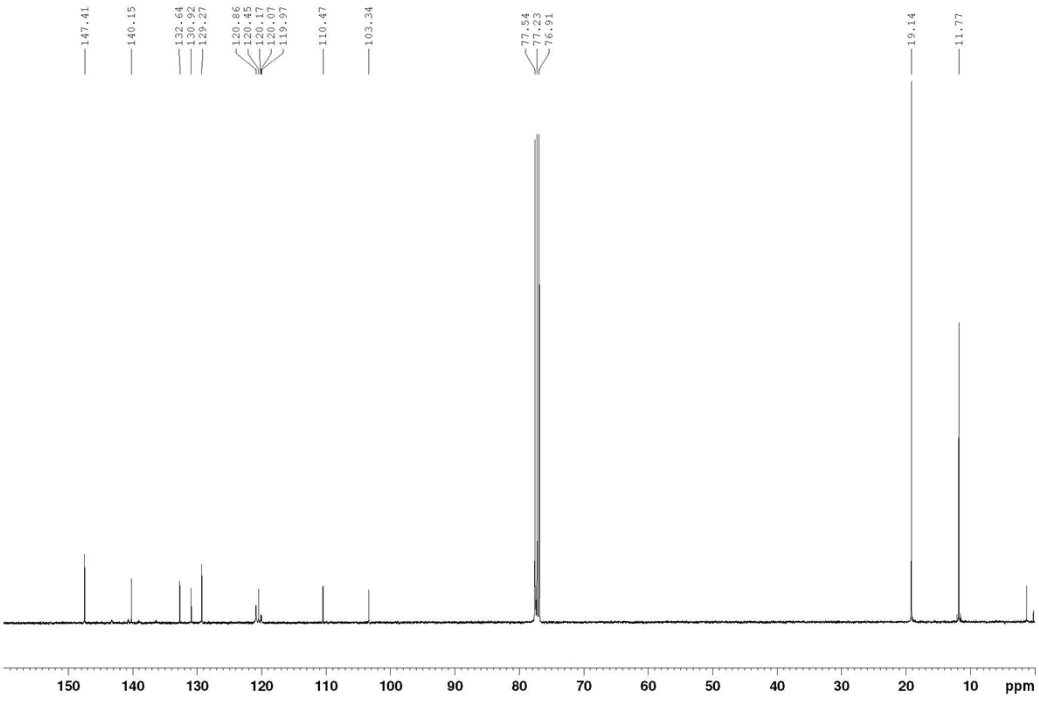

Mass spectra (MS)

Generic Display Report

Analysis Info

Analysis Name	D:\Data\YANGY_MS\New\LIUKE121126_5.d	Acquisition Date	11/27/2012 11:07:30
Method	APCIMS.m	Operator	ESQ6K
Sample Name	default	Instrument	esquire6000
Comment			

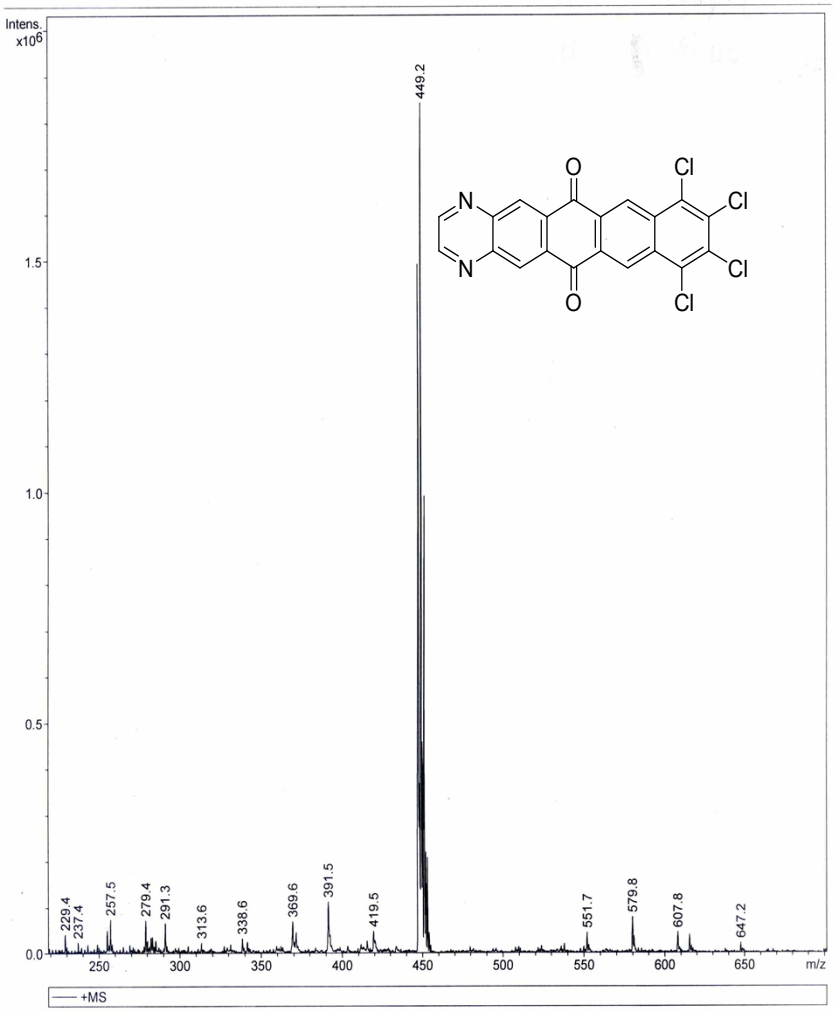

Generic Display Report

Analysis Info

Analysis Name	D:\Data\YANGY_MS\New\LIUKE121126_1.d	Acquisition Date	11/27/2012 10:45:00
Method	APCIMS.m	Operator	ESQ6K
Sample Name	default	Instrument	esquire6000
Comment			

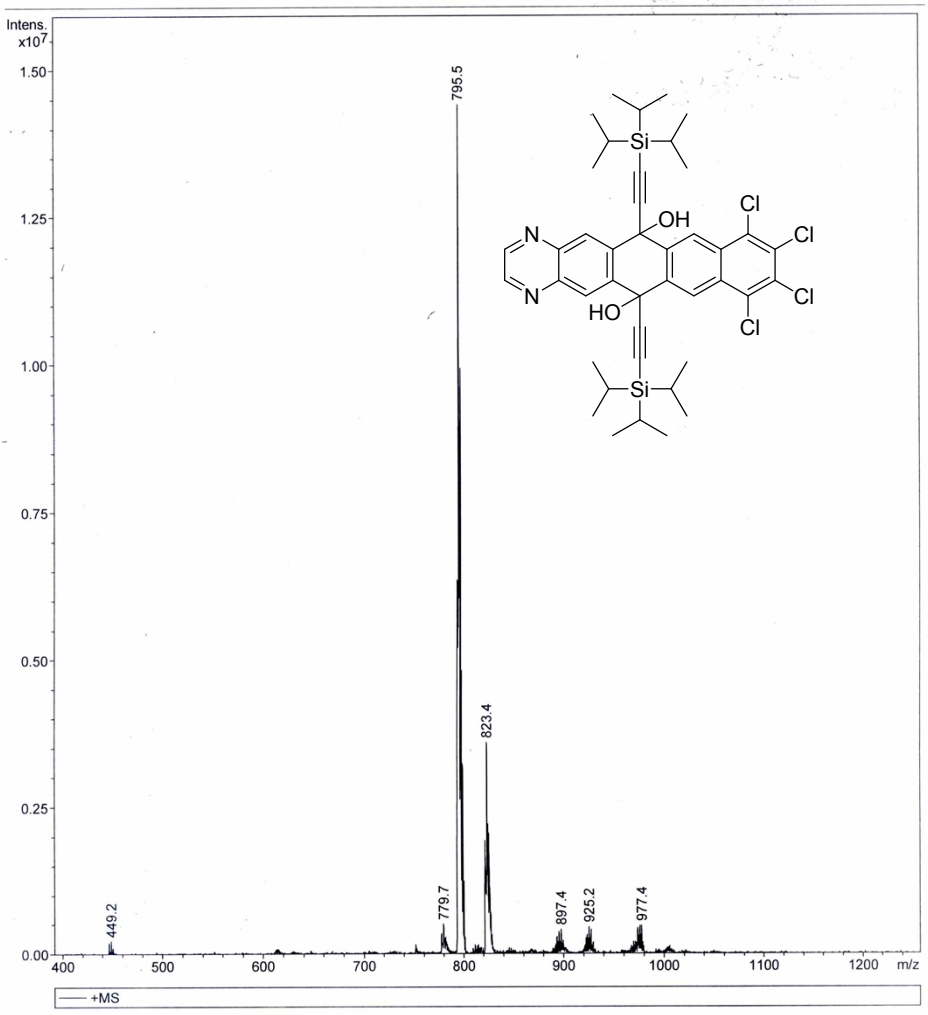

Bruker Daltonics DataAnalysis 3.4 printed: 11/27/2012 10:45:46 Page 1 of 1

Generic Display Report

Analysis Info

Analysis Name	D:\Data\YANGY_MS\New\LIUKE121126_3.d	Acquisition Date	11/27/2012 10:55:58
Method	APCIMS.m	Operator	ESQ6K
Sample Name	default	Instrument	esquire6000
Comment			

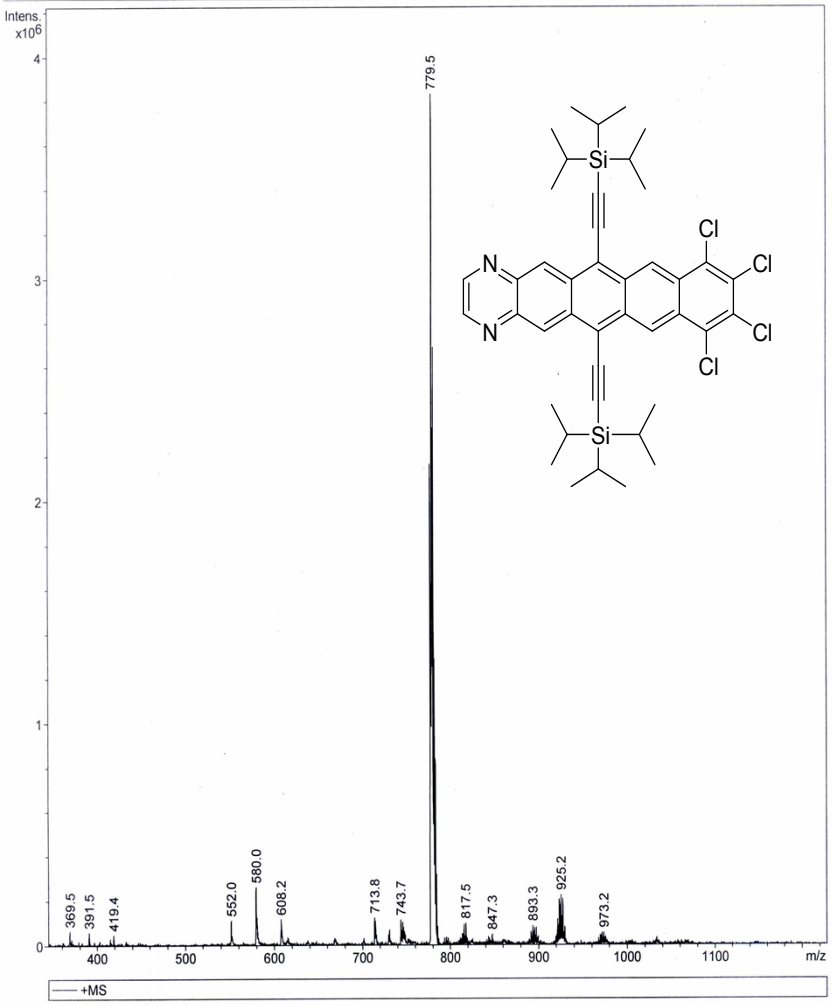

Generic Display Report

Analysis Info

Analysis Name	D:\Data\YANGY_MS\New\LIUKE121126_6.d	Acquisition Date	11/27/2012 11:13:02
Method	APCIMS.m	Operator	ESQ6K
Sample Name	default	Instrument	esquire6000
Comment			

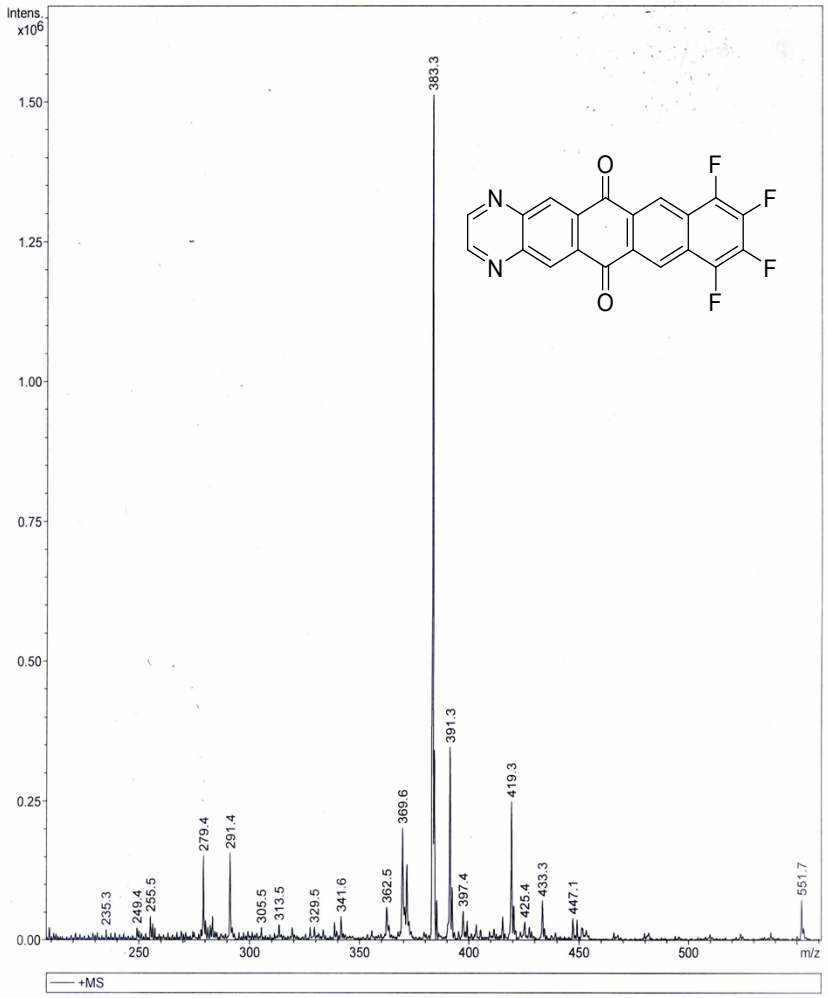

Generic Display Report

Analysis Info

Analysis Name	D:\Data\YANGY_MS\New\LIUKE121126_2.d	Acquisition Date	11/27/2012 10:50:49
Method	APCIMS.m	Operator	ESQ6K
Sample Name	default	Instrument	esquire6000
Comment			

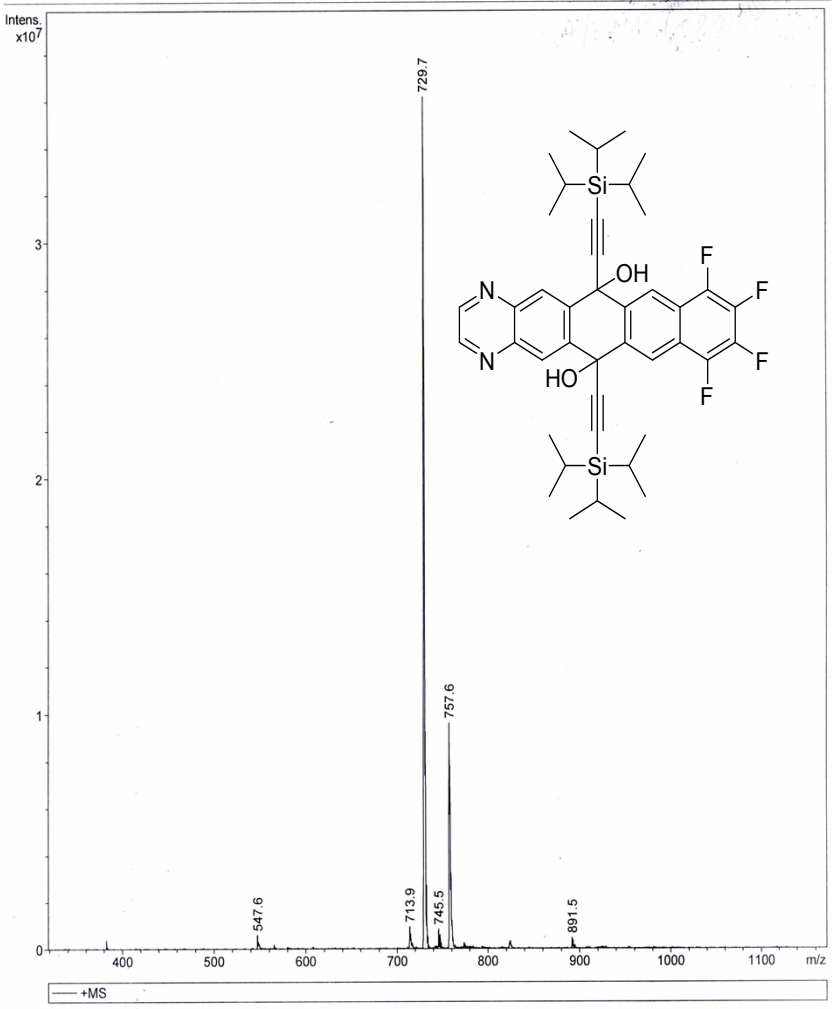

Bruker Daltonics DataAnalysis 3.4 printed: 11/27/2012 10:55:23 Page 1 of 1

Generic Display Report

Analysis Info

Analysis Name	D:\Data\YANGY_MS\New\LIUKE121126_4.d	Acquisition Date	11/27/2012 10:59:18
Method	APCIMS.m	Operator	ESQ6K
Sample Name	default	Instrument	esquire6000
Comment			

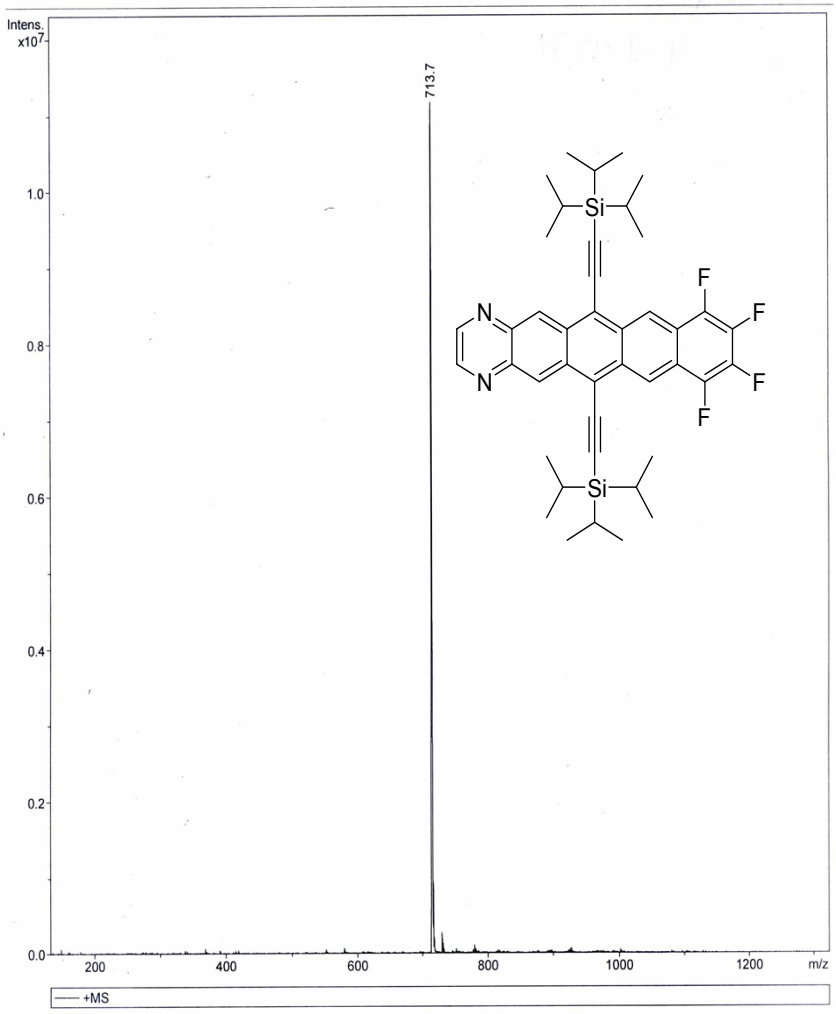

Bruker Daltonics DataAnalysis 3.4 printed: 11/27/2012 11:07:05 Page 1 of 1

9. References

1. J. E. Anthony, J. S. Brooks, D. L. Eaton and S. R. Parkin, *J. Am. Chem. Soc.*, 2001, 123, 9482.
2. Y.-Y. Liu, C.-L. Song, W.-J. Zeng, K.-G. Zhou, Z.-F. Shi, C.-B. Ma, F. Yang, H.-L. Zhang and X. Gong, *J. Am. Chem. Soc.*, 2010, 132, 16349.
3. C.-L. Song, C.-B. Ma, F. Yang, W.-J. Zeng, H.-L. Zhang and X. Gong, *Org. Lett.*, 2011, 13, 2880.
4. K. Senthilkumar, F. C. Grozema, F. M. Bickelhaupt and L. D. A. Siebbeles, *J. Chem. Phys.*, 2003, 119, 9809.
5. M. Winkler and K. N. Houk, *J. Am. Chem. Soc.*, 2007, 129, 1805.
6. M. C. R. Delgado, K. R. Pigg, D. A. d. S. Filho, N. E. Gruhn, Y. Sakamoto, T. Suzuki, R. M. Osuna, J. Casado, V. Hernández, J. T. L. Navarrete, N. G. Martinelli, J. Cornil, R. S. Sánchez-Carrera, V. Coropceanu and J.-L. Brédas, *J. Am. Chem. Soc.*, 2009, 131, 1502.
7. H. Geng, Y. Niu, Q. Peng, Z. Shuai, V. Coropceanu and J. L. Brédas, *J. Chem. Phys.*, 2011, 135, 104703.
8. W.-Q. Deng and I. William A. Goddard, *J. Phys. Chem. B*, 2004, 108, 8614.
9. C.-H. Li, C.-H. Huang and M.-Y. Kuo, *Phys. Chem. Chem. Phys.* , 2011, 13, 11148.
10. J.-L. Brédas, D. Beljonne, V. Coropceanu and J. Cornil, *Chem. Rev.*, 2004, 104, 4971.
11. G. Nan, X. Yang, L. Wang, Z. Shuai and Y. Zhao, *Phys. Rev. B*, 2009, 79, 115203.
12. X. Yang, L. Wang, C. Wang, W. Long and Z. Shuai, *Chem. Mater.*, 2008, 20, 3205.